

High-transmissivity Silicon Visible-wavelength Metasurface Designs based on Truncated-cone Nanoantennae

Krupali D. Donda, Ravi S. Hegde

*Department of Electrical Engineering,
Indian Institute of Technology, Gandhinagar, Gujarat, India, 382355
hegder@iitgn.ac.in*

Abstract

High-transmissivity all-dielectric metasurfaces have recently attracted attention towards the realization of ultra-compact optical devices and systems. Silicon based metasurfaces, in particular, are highly promising considering the possibility of monolithic integration with VLSI circuits. Realization of silicon based metasurfaces operational in the visible wavelengths remains a challenge. A numerical study of silicon metasurfaces based on stepped truncated cone shaped nanoantenna elements is presented. Metasurfaces based on the stepped conical geometry can be designed for operation in the 700nm to 800nm wavelength window and achieve full cycle phase response (0 to π with an improved transmittance in comparison with previously reported cylindrical geometry [1]. A systematic parameter study of the influence of various geometrical parameters on the achievable amplitude and phase coverage is reported.

Keywords: Metasurface, Nanoantenna, CMOS compatible, Integrated Optics, Theory and Simulation.

1. Introduction

The metasurface [2, 3, 4, 5, 6], a paradigm-shifting concept, promises the next-generation of flat, integrable devices for the manipulation of optical wavefronts. It is a spatially heterogeneous array of nanoscale resonant elements (called meta-atoms) that can in general alter the amplitude, phase, spectrum

and polarization values of an incident wavefront in a short propagation distance and with a sub-wavelength scale in the transverse plane [6]. The metasurface concept [7, 8] has been primarily explored in connection with plasmonic nanoantenna in the recent past [3]. Traditional plasmonic materials, however, are not compatible with the CMOS process flow, and, additionally, the high absorption [9] is problematic in transmission based applications [10]. Recently it was suggested to replace the plasmonic metals used for nanoantenna with high-index dielectrics resulting in the so called all-dielectric nanoantenna [11]. These nanoantenna do not strongly enhance the local electromagnetic field as do plasmonic nanoantenna, but they suffer far lower amounts of dissipative loss and offer magnetic response at higher frequencies [12, 13, 14, 15]. Dielectric nanoantenna have been traditionally studied in the microwave community as dielectric resonator antenna [16].

By using silicon based nanoantenna, reflectionless phase control of incident wavefront (Huygens' surface) in a transmissive metasurface was reported recently and offered a much higher efficiency in comparison to a plasmonic metasurface [17, 18, 19]. High index dielectric nanoantenna arrays can also be considered as two dimensional high-index contrast subwavelength diffraction gratings; various optical wavefront manipulation possibilities have been demonstrated with these so called HCTA (High Contrast Transmitarrays) [20, 21, 22, 23]. Most of these reports have been demonstrated at near IR operating wavelengths where they have achieved high transmission efficiencies. Scaling the operational wavelength of silicon metasurfaces into the visible region is attractive as they can be combined with silicon photodetectors and electronic postprocessing. Currently reported silicon metasurfaces using cylindrical nanoantenna as meta-atoms [1, 24] have seen worse performance in the visible region as compared to near IR region. It has been speculated that the higher material absorption losses of silicon and increased mutual coupling could limit its performance [1, 24] prompting researchers to look into other material systems like Titanium dioxide [1, 24].

While alternate semiconducting high-index materials are one pathway to-

wards realization of all-dielectric visible wavelength metasurfaces, silicon remains an attractive option particularly for chip-scale integration of metasurfaces. We propose here a bilayered stepped truncated conical geometry as the meta-atom and compare its performance with a simple cylindrical shape using silicon as the material. We show that the proposed design performs better than the cylindrical geometry in the visible wavelength window of 700nm to 800nm; however, this comes at the cost of added fabrication complexity. The truncated cone shape has been previously explored in connection with RF dielectric resonator antenna [25] and has been found to have several favorable properties including a wider operational bandwidth. The paper begins with a description and exploration of the spectral response of the proposed stepped cone nanoantenna in section 2. In section 3, the amplitude and phase response of this structure and the dependence on various geometrical parameters is described before concluding the paper in section 4.

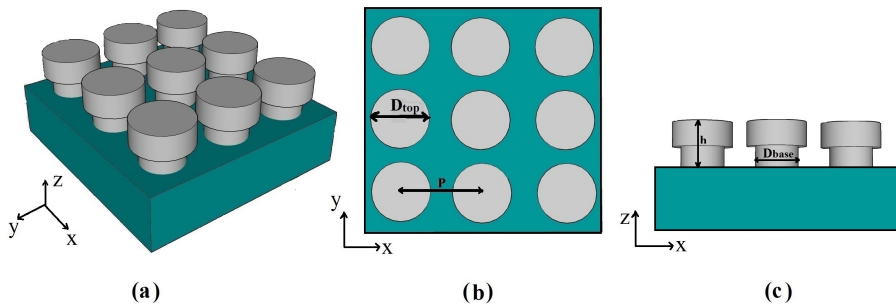


Figure 1: Schematic of the proposed inverted cone bilayer dielectric metasurface consisting of Silicon nanoantenna of total height h in air on a fused silica substrate with the various geometrical parameters labelled. (a), (b) and (c) show the perspective, top and side views respectively.

2. The stepped-conical silicon nanoantenna

2.1. Structure Description

The proposed bilayer dielectric metasurface consists of an array of heterogeneously sized nanoantennae arranged in a regular rectangular lattice. The

schematic shown in figure 1 can be thought of as a section of this spatially variant metasurface. The individual nanoantenna is shaped in the form of a truncated two stepped cone and is characterized by four geometrical parameters: the diameter of the top cone $D_{top} = 2R_{top}$, the diameter of the bottom cone $D_{bottom} = 2R_{bottom}$ and, the respective heights h_{top} and h_{bottom} . Throughout this paper, we consider a uniform rectangular lattice of periodicity P and heights h_{top} and h_{bottom} ; the diameters D_{top} and D_{bottom} are, however, free to change throughout the extent of the metasurface. Furthermore, we also restrict our attention to the case where the thickness of the metasurface or the total height h (equal to $h_{top} + h_{bottom}$) is 130nm. The height of 130nm was chosen so that the primary resonances occur in the red spectral range of 700nm to 800nm where intrinsic absorption loss of amorphous silicon is small [1].

The numerical simulations were performed with the Finite Element Method (FEM) based frequency solver in the commercial software suite CST Microwave studio. The extinction cross section calculation uses open boundaries on all sides with a plane wave illumination. The extinction cross sections are calculated by summing the scattering and the absorption cross sections. The scattering cross section is obtained by integrating the total scattered power by first generating the far fields using far field transformations applied to the near fields captured at the open boundaries. On the other hand, the reflectance and transmittance spectra for the array are obtained by using periodic boundary conditions and Floquet port excitation. Tabulated values reported in the literature were used to model the dispersive permittivity of silicon [26] and a constant refractive index of 1.45 is assumed for the silica substrate. The solver uses a tetrahedral meshing scheme, starts out with a step size of 4 per smallest simulation wavelength and a minimum of 10 for any given edge. The solver iteratively refines the mesh and converges to a final mesh geometry.

2.2. Optical response of stepped cone

The spectral response of a nanoscale resonator made of a high-index dielectric material is dominated by the magnetic and electric dipole resonances [27]

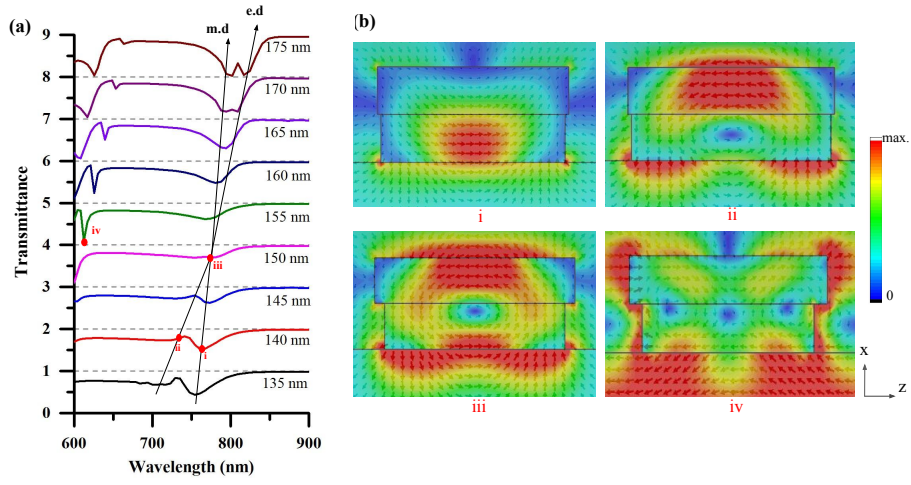


Figure 2: (a) Transmission spectra for the stepped conical dielectric nanoantenna geometry. The structure is excited with a normally incident plane wave illumination from the top (top radius is varying from <https://www.sharelatex.com/project/58ec81482836187d713d78d5> 145 nm to 175 nm and the base radius 135 nm is held constant). The total height h is 130 nm and periodicity P is $D_{top} + 115$. Guide lines are drawn that track the magnetic dipolar (md) and electric dipolar (ed) resonance wavelengths. (b) At 4 selected resonance wavelengths (marked (i), (ii), (iii) and (iv) in (a)), the near field plots of the electric field is shown for a $x - z$ cut of the structure.

that are induced in it by the incident field. This is seen most easily in the resonances of a spherical particle made of silicon (see figure S1). A formal mathematical treatment of the electromagnetic scattering behaviour of a spherical particle (reported by G. Mie in 1908 [28]) predicts the existence of magnetic dipole resonances [27]. In particular, for a spherical particle made of a high-refractive index material, the magnetic dipole frequency is lower in comparison to the electric dipole frequency [29]. For a spherical particle, the magnetic dipole resonance frequency occurs at the free space wavelength λ when $\lambda/n(\lambda)$, the wavelength in the particle equals the diameter of the particle $2R_s$ (here $n(\lambda)$ is the wavelength dependent refractive index of the scattering medium). The orientation of the electric field becomes exactly anti-parallel at the sphere boundaries at this condition resulting in a circulating induced current in it; the circulating current results in the magnetic dipole radiation and hence an increased scattering at this particular frequency. At the electric dipole resonance condition, the electric field lines exhibit behavior similar to that of an electric dipole (see figure S1).

A nanoantenna which is non-spherical also exhibits magnetic and electric dipolar modes. The numerical simulation results shown in figure S2 (b and c) clearly show the similarity of the magnetic dipolar resonance occurring in the case of the stepped cone structure and that of the nanosphere. In particular, the telltale sign is the presence of the circulating electric fields. In figure , various bilayered cones are considered with changing top radius. Widening the top radius redshifts both the magnetic and the electric dipolar resonances with the redshift of the electric dipolar resonances being much stronger. This causes a condition whereby both the resonances occur at the same wavelength (in this case occurring for $R_{top} = 150\text{nm}$ at the wavelength of 780nm. It has been reported that when such an overlap occurs, the backscattering is completely cancelled in favor of forward scattering [19]. Thus while the transmission drops at wavelengths where the magnetic and electric dipolar resonances individually, it is seen to peak when the resonances overlap.

3. Results and Discussion

3.1. Amplitude and phase response

Consider the transmission amplitude and phase response for the nanocone structure. Two variations are possible: inverted and straight lying nanocones with respect to the substrate. Figure 3 shows the transmittance (the amplitude transmission is squared to obtain the transmittance) and phase response (expressed in multiples of 2π) of inverted and straight cone structures respectively for wavelength range 600nm to 900nm. A full range of phase coverage is possible as noted in (b) with high transmission efficiency (a). Here, resonance is shifting towards lower frequencies linearly with increase in the top diameter. The optimal transmission case is reached for top radius of 145 nm with peak transmission $\geq 95\%$. In case of straight cone, it is observed that the overall transmission is poorer than that for inverted stepped cone. Furthermore, a full phase coverage is possible for a wider range of sizes for the inverted cone. The inverted orientation is thus considered throughout this article for systematic investigation.

While the nanocylinder also achieves a full phase coverage range, the inverted nanocone outperforms the cylinder in terms of the transmittance as seen in figure ???. Two sets of data are plotted: each set considers shapes with a constant base radius but changing top radius. It is seen that the nanocone performs better than the cylinder in each case.

3.2. Influence of geometric parameters

This section discusses the influence of various geometrical parameters on the response of the inverted nanocone; specifically, the influence of inter-antenna spacing, height ratios and uniform geometrical scaling. As seen in figure (a), as the periodicity increases, the main resonant dip is slightly shifted toward lower frequencies from 750nm to 800nm and a narrow spectral feature, arising out of another resonance is created in the wavelength region of 600nm and 650nm. Periodicity values of 400nm to 450nm are seen to provide the highest

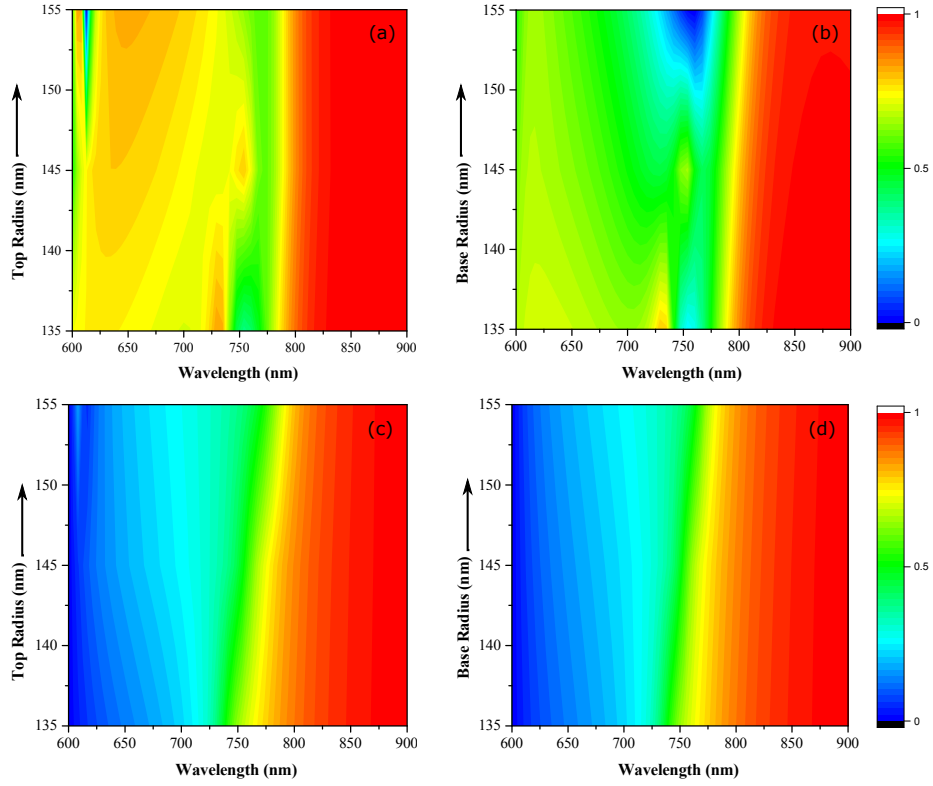


Figure 3: (a,c) Transmittance and phase response of inverted nanocone. Base radius is fixed at 135nm and top radius is changing from 135nm to 155nm. (b,d) Transmittance and phase response of straight nanocone. Top radius is fixed at 135nm and base radius is changing from 135nm to 155nm. The total height h is 130nm and periodicity P is $D_{top} + 115$ nm.

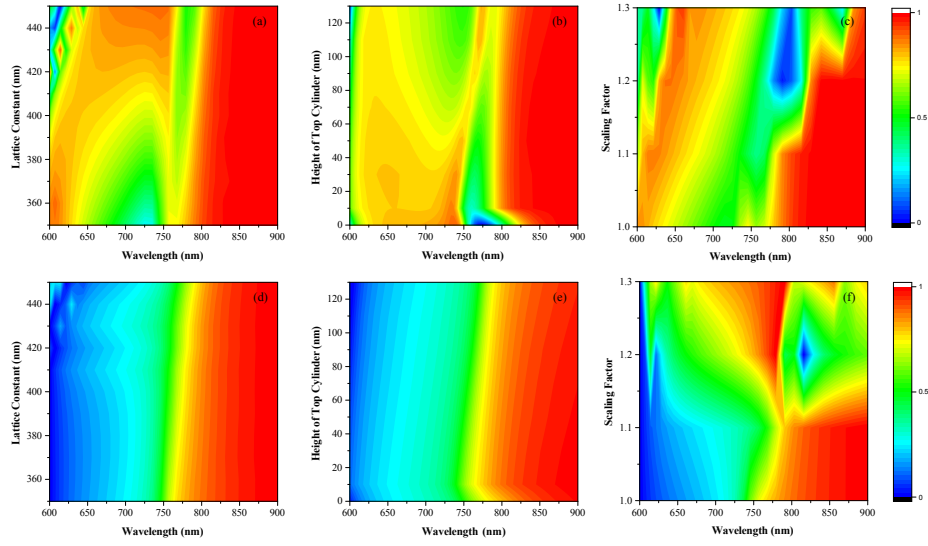


Figure 4: (a,d) Transmittance and phase response of inverted nanocone with base radius 135nm and top radius 145nm for variation in the inter-antenna spacing. The heights h_{top} and h_{bottom} are equal and the total height h is 130nm. (b,e) Transmittance and phase response of inverted nanocone with base and top radius and total height same as in (a, d) but with varying h_{top} . (c,f) Transmittance and phase response of inverted nanocone when all the geometric properties $P, D_{top}, D_{bottom}, h_{top}$ and h_{bottom} are scaled uniformly. The scaling factor 1 denotes the case of base radius 135nm and top radius 145nm, h is 130nm and periodicity 405nm.

overall transmittance. Phase coverage, however, is seen to be unaffected with periodicity change as seen in figure (b). As seen in figure (b), a height ratio of 1:1 is seen to provide the best overall transmittance. Again, the phase coverage is not strongly influenced by this factor as seen in figure (e). Uniform scaling of the nanocone is expected to shift the operating wavelength to a higher wavelength. However, unexpectedly, this expectation is not borne out by the results seen in figure (c) and (f).

3.3. Metasurface design at a specific wavelength

The optimal transmission case is reached for top radius of 145 nm and base radius of 135 nm with peak transmission $\geq 95\%$ at the wavelength of 770nm as can be seen in figure 3. At this wavelength, a precise overlap of the electric and magnetic dipole resonances occurs and leads to near unity transmission and zero reflection Huygens surface [19]. To design a metasurface with a full phase control at this specific wavelength, we can vary the geometrical parameters around the optimal combination [1]. Note that as the geometrical parameters change to provide a particular phase, the transmittance value may drop from the peak value. Figure 5 shows the transmittance and phase response for various combinations of geometrical parameters for the inverted truncated cone. The overall device efficiencies reported, for instance, in a nanocylinder based metasurface beam deflector is around 45% [1]. The addition of a second geometrical parameter makes it possible to optimally pick geometrical parameters to maximize the transmittance at any given phase angle. This will lead to improvement of overall device efficiency.

The transmittance and phase response changes for a shift in the operational wavelength decides the operational bandwidth of the metasurface device. From figure 5, we see that the total operational bandwidth is indeed quite limited. Yu and coworkers [1] report on a peculiar observation that experimentally observed transmittance is better than the simulated ones. In the simulations, it is observed that the magnetic dipole resonance is fairly broader in comparison with the electrical case, and, furthermore, that the electrical resonance is less

spatially confined. This decreases the overall spectral overlap between the magnetic and dipole resonances. In experimental studies, various non-idealities serve to broaden the electric dipole resonance. Thus, the operational bandwidth is expected to be better than that observed in simulations.

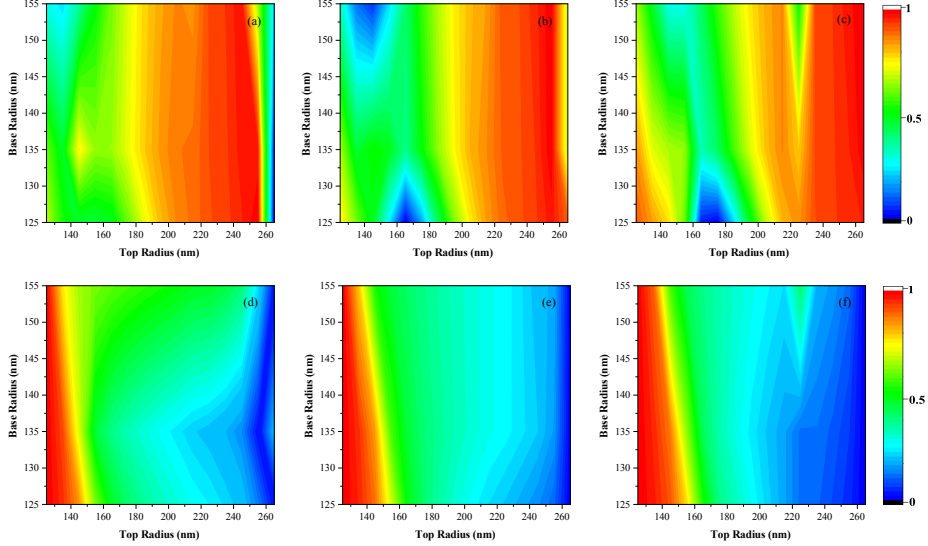


Figure 5: Transmittance and Phase response for various combinations of base and top radii at the wavelength of 770nm where there is the best overlap of the magnetic and electric dipole resonances. Comparison with nearby wavelengths is also shown. (b,e) transmittance and phase response at 770nm, (a,d) 760nm and (c,f) 780nm. Height h is 760nm and the periodicity $P = D + 115$

4. Conclusion

A design modification is proposed for nanocylinder based silicon dielectric metasurfaces that can improve their overall transmission efficiencies for visible-wavelength operation. The efficiency improvement however requires the fabrication of two aligned layers. We note, however, that several workers have already reported metasurfaces that use a bilayered geometry [30, 31, 32] with requirement of precise nanoscale alignments requirements between the two layers. The most directly relevant reported structures are the so called “mush-

room” nanopillars [33, 34, 35]. By the use of a sacrificial layer [33], the second layer can be fabricated (see figure S3). Fabrication of the bilayer metasurface could potentially lead to misalignment in the two component cylinders. We have studied the effect on transmittance and phase response due to misalignment of top cylinder with respect to bottom cylinder (see figure S4). The misalignment leads to a translation of one center with respect to the other. For small offsets of up to 25nm, there is a negligible alteration in the transmittance and phase response.

Future studies can consider other non-symmetrical geometries. Although, the reported metasurface design allows a wider simultaneous control of amplitude and phase; not all possible combinations are obtained. We are investigating other geometries to allow fully arbitrary selection of both phase and amplitude change. The numerical study assumes the unit-cell approach whereby the mutual coupling between neighboring elements is assumed to be negligible. The mutual coupling effect is expected to become more dominant as the wavelength is further reduced below 700nm. Thus the reported designs may not scale below 700nm. Future studies will investigate the influence of mutual coupling and devise design strategies that take these into consideration.

Acknowledgment

The authors acknowledge support from the Department of Science and Technology, Govt. of India through the Extramural grant SB/S3/EECE/0200/2015.

REFERENCES

References

- [1] Ye Feng Yu, Alexander Y. Zhu, Ramón Paniagua-Domínguez, Yuan Hsing Fu, Boris Luk'yanchuk, and Arseniy I. Kuznetsov. High-transmission dielectric metasurface with 2π phase control at visible wavelengths. *Laser and Photonics Reviews*, 9(4):412–418, 2015.

- [2] Patrice Genevet and Federico Capasso. Holographic optical metasurfaces: a review of current progress. *Reports on progress in physics. Physical Society (Great Britain)*, 78(2):024401, 2015.
- [3] Nikolay I. Zheludev and Yuri S. Kivshar. From metamaterials to metadevices. *Nature Materials*, 11(11):917–924, 2012.
- [4] D. Lin, P. Fan, E. Hasman, and M. L. Brongersma. Dielectric gradient metasurface optical elements. *Science*, 345(6194):298–302, 2014.
- [5] Nina Meinzer, William L Barnes, and Ian R Hooper. Plasmonic meta-atoms and metasurfaces. *Nature Photonics*, 8(12):889–898, 2014.
- [6] Alexander E. Minovich, Andrey E. Miroshnichenko, Anton Y. Bykov, Tatiana V. Murzina, Dragomir N. Neshev, and Yuri S. Kivshar. Functional and nonlinear optical metasurfaces. *Laser and Photonics Reviews*, 9(2):195–213, 2015.
- [7] Nanfang Yu, Patrice Genevet, Mikhail a Kats, Francesco Aieta, Jean-Philippe Tetienne, Federico Capasso, and Zeno Gaburro. Light Propagation with Phase Discontinuities: Generalized Laws of Reflection and Refraction. *Science*, 334:333–337, 2011.
- [8] Nanfang Yu and Federico Capasso. Flat optics with designer metasurfaces. *Nature Materials*, 13(2):139–150, 2014.
- [9] Jacob B. Khurgin. How to deal with the loss in plasmonics and metamaterials. *Nature Nanotechnology*, 10(1):2–6, 2015.
- [10] Francesco Aieta, Patrice Genevet, Mikhail a. Kats, Nanfang Yu, Romain Blanchard, Zeno Gaburro, and Federico Capasso. Aberration-free ultrathin flat lenses and axicons at telecom wavelengths based on plasmonic metasurfaces. *Nano Letters*, 12(9):4932–4936, 2012.
- [11] Andrey E. Miroshnichenko. All-dielectric optical nanoantennas. In Dr. Laure Huitema, editor, *IEEE Antennas and Propagation Society, AP-S*

International Symposium (Digest), volume 2015-October, chapter 6, pages 601–602. 2015.

- [12] Andrey E. Miroshnichenko, Ivan S. Maksymov, Arthur R. Davoyan, Constantin Simovski, Pavel Belov, and Yuri S. Kivshar. An arrayed nanoantenna for broadband light emission and detection. *Physica Status Solidi - Rapid Research Letters*, 5(9):347–349, 2011.
- [13] Alexander Krasnok, Stanislav Glybovski, Mihail Petrov, Sergey Makarov, Roman Savelev, Pavel Belov, Constantin Simovski, and Yuri Kivshar. Large Purcell enhancement without strong field localization. *arXiv*, pages 1–6, 2015.
- [14] Alexander E Krasnok, Constantin R Simovski, Pavel a Belov, and Yuri S Kivshar. Superdirective dielectric nanoantennas. *Nanoscale*, 6(13):7354–61, 2014.
- [15] a E Krasnok, I S Maksymov, a I Denisyuk, P a Belov, a E Miroshnichenko, C R Simovski, and Yu S Kivshar. Optical nanoantennas. *Physics-Uspokhi*, 56(6):539–564, 2013.
- [16] Km Luk and Kw Leung. *Dielectric resonator antennas*. Research Studies Press Ltd., 2003.
- [17] Salvatore Campione, Lorena I. Basilio, Larry K. Warne, and Michael B. Sinclair. Tailoring dielectric resonator geometries for directional scattering and Huygens metasurfaces. *Optics Express*, 23(3):2293, 2015.
- [18] Manuel Decker, Isabelle Staude, Matthias Falkner, Jason Dominguez, Dragomir N. Neshev, Igal Brener, Thomas Pertsch, and Yuri S. Kivshar. High-Efficiency Dielectric Huygens’ Surfaces. *Advanced Optical Materials*, 3(6):813–820, 2015.
- [19] Isabelle Staude, Andrey E. Miroshnichenko, Manuel Decker, Nche T. Fofang, Sheng Liu, Edward Gonzales, Jason Dominguez, Ting Shan Luk,

- Dragomir N. Neshev, Igal Brener, and Yuri Kivshar. Tailoring directional scattering through magnetic and electric resonances in subwavelength silicon nanodisks. *ACS Nano*, 7(9):7824–7832, 2013.
- [20] a Arbabi, Y Horie, M Bagheri, and a Faraon. Dielectric metasurfaces for complete control of phase and polarization with subwavelength spatial resolution and high transmission. *Nat Nanotechnol*, 10(11):937–943, 2015.
- [21] Amir Arbabi, Yu Horie, Alexander J Ball, Mahmood Bagheri, and Andrei Faraon. Subwavelength-thick Lenses with High Numerical Apertures and Large Efficiency Based on High Contrast Transmitarrays. *Nature communications*, 6(May):1–10, 2015.
- [22] Ehsan Arbabi, Amir Arbabi, Seyedeh Mahsa Kamali, Yu Horie, and Andrei Faraon. Multiwavelength polarization insensitive lenses based on dielectric metasurfaces with meta-molecules. *Optica*, 0(6):1–12, 2016.
- [23] Amir Arbabi, Yu Horie, Alexander J. Ball, Mahmood Bagheri, and Andrei Faraon. Efficient high NA flat micro-lenses realized using high contrast transmitarrays. In *Spie Opto*, volume 9372, page 93720P, 2015.
- [24] M. Khorasaninejad, W. T. Chen, R. C. Devlin, J. Oh, a. Y. Zhu, and F. Capasso. Metalenses at visible wavelengths: Diffraction-limited focusing and subwavelength resolution imaging. *Science*, 352(6290):1190–1194, 2016.
- [25] Ahmed a. Kishk, Yan Yin, and a. W. Glisson. Conical dielectric resonator antennas for wide-band applications. *IEEE Transactions on Antennas and Propagation*, 50(4):469–474, 2002.
- [26] EDWARD D. PALIK. *Handbook of Optical Constants of Solids*, volume 2. Academic Press, Boston, 1991.
- [27] Andrey E. Miroshnichenko. All-dielectric optical nanoantennas. In Laure Huitema, editor, *IEEE Antennas and Propagation Society, AP-S International Symposium (Digest)*, volume 2015-October, chapter 6, pages 601–602. InTech, 2015.

- [28] Gustav Mie. Beiträge zur Optik trüber Medien, speziell kolloidaler Metallösungen. *Annalen der Physik*, 330(3):377–445, 1908.
- [29] Dmitry Permyakov, Ivan Sinev, Dmitry Markovich, Pavel Ginzburg, Anton Samusev, Pavel Belov, Vytautas Valuckas, Arseniy I Kuznetsov, Boris S Luk, Andrey E Miroshnichenko, Dragomir N Neshev, and Yuri S Kivshar. Probing magnetic and electric optical responses of silicon nanoparticles. *Applied Physics Letters*, 171110:1–4, 2015.
- [30] Naoya Tate, Hiroki Sugiyama, Makoto Naruse, Wataru Nomura, Takashi Yatsui, Tadashi Kawazoe, and Motoichi Ohtsu. Quadrupole-dipole transform based on optical near-field interactions in engineered nanostructures. *Optics express*, 17(13):11113–21, 2009.
- [31] Richard Taubert, Mario Hentschel, Jürgen Kästel, and Harald Giessen. Classical analog of electromagnetically induced absorption in plasmonics. *Nano Letters*, 12(3):1367–1371, 2012.
- [32] R Bott. Hybrid bilayer plasmonic metasurface efficiently manipulates visible light. *Igarss 2014*, (1):1–5, 2014.
- [33] Y Ding Y Wang, H Hu, J Shao. Fabrication of well-defined mushroom-shaped structures for biomimetic dry adhesive by conventional photolithography and molding. *ACS applied materials & interfaces*, 6(4):2213–2218, 2014.
- [34] Ebrahim Forati and Dan Sevenpiper. Fabrication recipe for nanoscale suspended gold structures such as mushrooms and air bridges used in optical metasurfaces. *Journal of the Optical Society of America B*, 33(2):A61–A65, 2016.
- [35] Seong Min Kang. Role of wide tip of mushroom-like micropillar arrays to make the Cassie state on superrepellent surfaces. *RSC Adv.*, 6(78):74670–74674, 2016.